Angewandte Chemie
Eine Zeitschrift der Gesellschaft Deutscher Chemiker

Supporting Information

69451 Weinheim, Germany

The S_2 State of the Oxygen-Evolving Complex of Photosystem II Explored by QM/MM Dynamics: Spin Surfaces and Metastable States Suggest a Reaction Path Towards the S_3 State**

*Daniele Bovi, Daniele Narzi, and Leonardo Guidoni**

anie_201306667_sm_miscellaneous_information.pdf

Supporting Information

Computational details

QM/MM. Our QM/MM computational setup was based on the recent crystal structure at 1.9 Å resolution[1] of PSII (PDB ID: 3ARC). We treated at DFT+U level a portion of the system consisting of 202 atoms, including the Mn_4CaO_5 cluster, the side chains of its coordinating protein residues (Asp170, Glu189, His332, Glu333, Asp342, Ala344, and CP43-Glu354), the 14 closest water molecules plus other neighbouring amino acids (Asp61, Tyr161, Ser169, His190, His337, CP43-Arg357). We include in the classical system the D1, D2 and CP43 protein chains and the cofactors present in the respective domains. As starting positions for both models S_2^A and S_2^B of the Mn_4CaO_5 cluster we used the coordinates reported by Pantazis *et al*.[2]. The AMBER99SB force field[3] was used to describe the protein residues whereas the Generalised Amber Force Field (GAAF)[4] for the non standard residues and the lipids (i.e. β -carotene, chlorophyll a, pheophytin a, plastoquinone 9, heptyl 1-thiohexopyranoside, dodecyl- β -D-maltoside and the four lipids DGDG, MGDG, PG and SQDG). Partial charges of all the above mentioned molecules were calculated with the restrained electrostatic potential method.[5] For the description of the interactions between the QM and MM systems we used the efficient multigrid electrostatic coupling scheme from Laino *et al*.[6] as implemented in CP2K package.[7]

All QM/MM calculations were carried out within a DFT+U scheme[8,9,10] for the QM part, employing the functional PBE[11] with U* = 1.16 eV for the Hubbard correction. This value was extrapolated from preliminary calculations (not shown), comparing the exchange coupling constants (J_{ij}) obtained using different U values with that ones in which B3LYP functional was employed. The U* value was found to reproduce the exchange interactions between the magnetic electrons on the manganese ions for the two studied systems (S_2^A and S_2^B models) in agreement with the results obtained by Pantazis *et al*.[2]. For both QM/MM geometry optimizations and molecular dynamics the electronic structure was described by (UKS) DFT+U calculations, using the CP2K package with the Gaussian and plane-wave (GPW) method[7]. We used the MOLOPT-DZVP basis set, advised for fast and accurate calculations on molecular dynamics[12] in combination with GTH pseudopotentials[13, 14]. The kinetic energy cutoff for the plane-wave basis set was set to 380 Rydberg for the geometry optimization calculations and to 280 Rydberg for the MD simulations. The broken-symmetry states used to describe the properties of different spin surfaces and the exchange coupling constants were obtained by setting the appropriate initial guesses for the wave functions.

The QM/MM MD were performed in NVT ensemble at the temperature of 298 K, using the Nosé-Hoover thermostat[15,16,17] to couple the system with a double thermal bath (i.e. MM system and QM system), with a coupling constant τ = 0.1 ps. The Velocity-Verlet algorithm, with a time step of 0.5 fs, was employed. Procedural details on the performed QM/MM calculations can be found in the *Simulations* section (see below).

Free energy calculations

Free Energies were calculated by thermodynamic integration along the QM/MM molecular dynamics in canonical ensemble (NVT) at room temperature.
In order to evaluate the derivative of free energy over the reaction coordinate ξ, we estimated the ensemble-averaged force along the path direction. The relationship between the free energy difference and this force is shown by the following equation:

$$F(\xi_1) - F(\xi_0) = \int_{\xi_0}^{\xi_1} d\xi' \frac{\partial F(\xi')}{\partial \xi'} = \int_{\xi_0}^{\xi_1} d\xi' \left\langle \frac{\partial U(\xi')}{\partial \xi'} \right\rangle_{\xi'} = -\int_{\xi_0}^{\xi_1} d\xi' \, \langle f_{\xi'} \rangle_{\xi'}$$

where U(ξ) is the potential energy, $<\ldots>_{\xi}$ is the ensemble average with fixed ξ and f_{ξ} is the force along the reaction coordinate.

In the present work, in order to obtain the free energy description of the transition between the S_2^A and S_2^B structures of the Mn_4CaO_5 cluster, we define as reaction coordinate the difference of distances:

$$\xi = d(\mathrm{Mn4}, \mathrm{O5}) - d(\mathrm{Mn1}, \mathrm{O5})$$

where

$$d(\mathrm{Mn4}, \mathrm{O5}) = |\mathbf{r}_{\mathrm{Mn4}} - \mathbf{r}_{\mathrm{O5}}|$$
$$d(\mathrm{Mn1}, \mathrm{O5}) = |\mathbf{r}_{\mathrm{Mn1}} - \mathbf{r}_{\mathrm{O5}}|$$

As already shown in previous works[18,19,20], it is possible to calculate the statistical average force along the reaction coordinate by time average over molecular dynamics trajectories. The average force along the reaction coordinate has been calculated using the Lagrange multipliers technique[21-25] as

$$\langle f_{\xi'} \rangle_{\xi'} = \langle \lambda \rangle_{\xi'}.$$

where f is the force and λ the Lagrange multiplier.
The free energy is then reconstructed by numerical integration of the force as shown in the first equation of this section.

Broken symmetry approach

An accurate description of electronic states of multi-centre transition metal complexes require the use of a multireference approach, such as multireference configuration interaction or multireference coupled cluster.[26] Nevertheless, due to the excessive computational cost of these methods, a single determinant approach, such as Density Functional Theory (DFT) in Broken-Symmetry approach[27], is usually applied in the study of these systems. In particular, these scheme has been successfully applied for the description of the magnetic properties of di-manganese compounds. [28]

The possible BS states describing the electron density of the Mn_4CaO_5 cluster in S_2 state is reported in Table S1.

		S_2^A	S_2^B
BS state	S_z	$\|m_1, m_2, m_3, m_4\rangle$	$\|m_1, m_2, m_3, m_4\rangle$
Ψ_1	$13/2$	$\|+2, +3/2, +3/2, +3/2\rangle$	$\|+3/2, +3/2, +3/2, +2\rangle$
Ψ_2	$7/2$	$\|+2, -3/2, +3/2, +3/2\rangle$	$\|-3/2, +3/2, +3/2, +2\rangle$
Ψ_3	$7/2$	$\|+2, +3/2, -3/2, +3/2\rangle$	$\|+3/2, -3/2, +3/2, +2\rangle$
Ψ_4	$7/2$	$\|+2, +3/2, +3/2, -3/2\rangle$	$\|+3/2, +3/2, -3/2, +2\rangle$
Ψ_5	$5/2$	$\|-2, +3/2, +3/2, +3/2\rangle$	$\|+3/2, +3/2, +3/2, -2\rangle$
Ψ_6	$1/2$	$\|+2, -3/2, -3/2, +3/2\rangle$	$\|+3/2, -3/2, -3/2, +2\rangle$
Ψ_7	$1/2$	$\|+2, -3/2, +3/2, -3/2\rangle$	$\|-3/2, +3/2, -3/2, +2\rangle$
Ψ_8	$1/2$	$\|+2, +3/2, -3/2, -3/2\rangle$	$\|-3/2, -3/2, +3/2, +2\rangle$

Tab. S1: Broken symmetry spin states associated to $\mathbf{S_2^A}$ and $\mathbf{S_2^B}$ states of the Mn_4CaO_5 cluster.

In Figure S1 and below, we will refer to *A* and *B* as the direction of the spin (Up and Down) for the Mn(III) ions, whereas *a* and *b* will represent the direction of the spin (Up and Down) for the Mn(IV) ions.

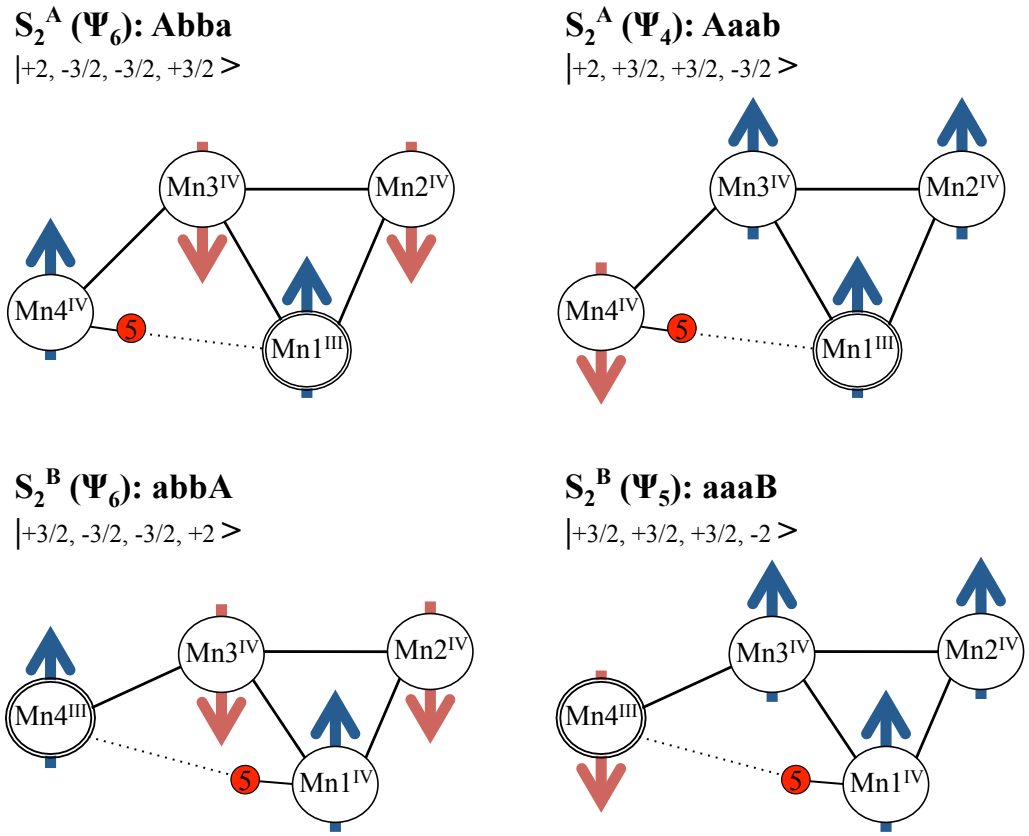

Fig. S1: Low Spin ($\Psi_6^A;\Psi_6^B$) and High Spin ($\Psi_4^A;\Psi_5^B$) broken symmetry states for $\mathbf{S_2^A}$ and $\mathbf{S_2^B}$ models. The oxygen O5 is also shown as a red circle.

Simulations

Several QM/MM simulations were carried out:

1) **S_2^A LS.** Starting from the PSII MM dynamics based on the X-ray structure by Umena *et al.*[1], we replaced the Mn_4CaO_5 cluster coordinates with the coordinates of the S_2^A optimized structure reported by D. A. Pantazis *et al.*[2]. After a QM/MM re-optimization of the structure in the LS-1/2 (Abba) state, we started the QM/MM MD at T = 298K in NVT ensemble. The first 2.5 ps of MD were used for thermalization whereas the following 12.5 ps were employed for data analysis.
2) **S_2^B HS-5/2**. The same procedure adopted for the S_2^A LS was employed in this case, using as starting structure the S_2^B optimized structure reported in Ref.[2] and re-optimized in the HS-5/2 (aaaB) state.
3) **Free Energy - LS**. To guarantee a smooth convergence we calculated the average force using 35 different ξ values, ranging from ξ= -1.5Å to ξ=+1.5Å. For all the 35 points along the reaction coordinate ξ distinct QM/MM MD were performed. After 2.0 ps of equilibration MD, the force for each ξ value was calculated averaging over an additional 1.5 ps of dynamics. The Free-Energy was derived integrating the force f_ξ along the reaction path using the trapezoidal rule.
4) **Free Energy – HS-5/2 and HS-7/2.** To evaluate the Free-Energy shape of the high-spin state characterized by the manganese spins arrangement Up-Up-Up-Down along the entire reaction path, we had to consider two different BS states because of the change of the Mn ions oxidation states in the two models (Fig.S1). Such spin state can be described in S_2^B by the state with S_z=5/2, the HS-5/2 aaaB (Mn4[III]), while in S_2^A by the state with S_z=7/2, the HS-7/2 Aaab (Mn1[III]). Accordingly this, we calculated the free energy in the same way as for the LS surface, but by dividing the path into two halves, each one described with the appropriate spin state. The energy differences between the minima of the two HS curves and the respective LS surface minima were adjusted in agreement with the energy values found in the QM/MM optimized geometries.

Geometrical parameters of the Mn_4CaO_5 cluster

The structural stability of the S_2^A and the S_2^B states was analyzed calculating the average distances and angles between the Mn_4CaO_5 atoms along the two QM/MM molecular dynamics trajectories. Analysis were performed on 15 ps trajectories neglecting the first 2.5 ps necessary for the thermal equilibration of the system. The calculated values are reported in Tab. S2 and compared with the respective values computed on the two optimized structures.

QM/MM	S_2^A LS		S_2^B HS	
	OPT	MD	OPT	MD
	Bond Distances (Å)			
Mn1-Mn2	2.76	2.79 (0.06)	2.77	2.78 (0.06)
Mn1-Mn3	3.34	3.36 (0.11)	2.94	2.94 (0.07)
Mn2-Mn3	2.78	2.81 (0.06)	2.77	2.81 (0.06)
Mn3-Mn4	2.77	2.77 (0.06)	3.09	3.15 (0.11)
Mn1-Ca	3.56	3.60 (0.12)	3.40	3.40 (0.11)
Mn2-Ca	3.38	3.41 (0.12)	3.45	3.43 (0.12)
Mn3-Ca	3.46	3.57 (0.14)	3.36	3.45 (0.14)
Mn4-Ca	3.64	3.81 (0.13)	3.79	3.99 (0.15)
Mn1-O5	2.98	3.08 (0.20)	1.86	1.88 (0.07)
Mn4-O5	1.87	1.87 (0.06)	3.07	3.13 (0.17)
Mn1-Mn4	4.82	4.89 (0.18)	4.93	5.00 (0.17)
	Angles degree			
Mn3-oxo-Mn4	96.25/97.79	95.9/96.7 (3.1/3.1)	115.63	117.5 (6.1)
Mn1-oxo-Mn2	96.28/91.63	98.1/92.2 (3.2/3.1)	96.17/93.19	97.6/92.6 (3.1/3.0)
Mn1-oxo-Mn3	116.00	116.8 (5.8)	103.11/97.99	102.2/97.5 (3.5/3.5)
Mn2-oxo-Mn3	98.51/90.36	99.1/90.4 (3.1/3.1)	98.12/90.82	99.4/90.9 (3.2/3.0)

Tab. S2: Geometrical values of the QM/MM optimized geometries (OPT) and average values along the QM/MM dynamics (MD). Standard deviations are reported in brackets.

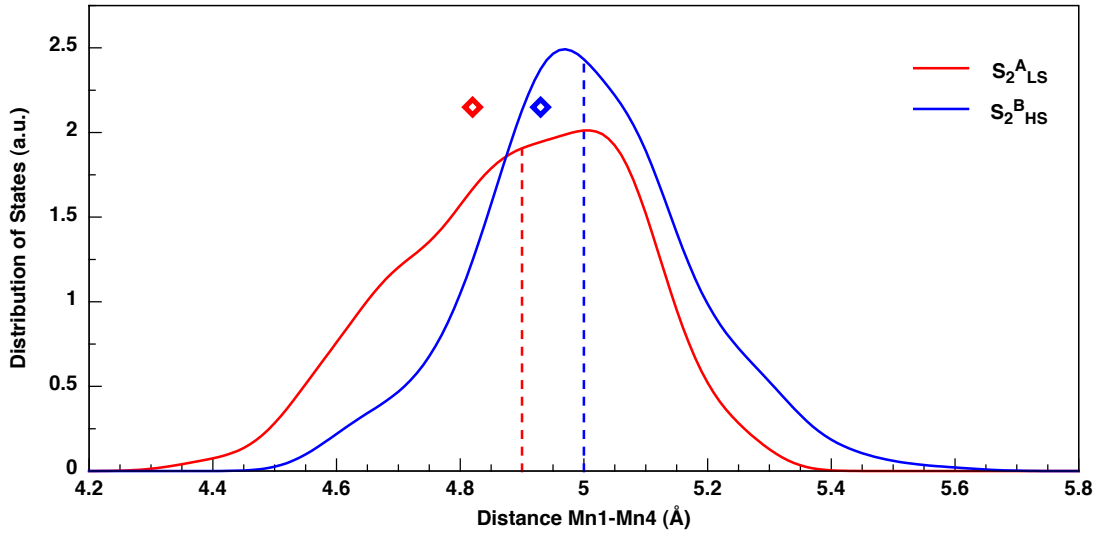

Fig. S2: Distributions of the distance between Mn1 and Mn4 obtained by 12.5 ps of room temperature QM/MM dynamics for both S_2^A in Low-Spin state (red line) and S_2^B in High-Spin state (blue line). The dashed lines show the average values, while the diamonds represent the distances calculated on the QM/MM optimized geometries.

Coordination numbers

The coordination numbers for Mn1 and Mn4 reported in Figure 2b were taken as the number of oxygen and nitrogen atoms within the first coordination shell, determined by the cumulative radial distribution function of these atoms around the respective manganese ions within a cut-off radius of 2.4 Å.

References to Supporting Information

1. Y. Umena, K. Kawakami, J.-R. Shen, N. Kamiya, *Nature* **2011**, *473*, 55 – 60

2. D. A. Pantazis, W. Ames, N. Cox, W. Lubitz, F. Neese, *Angew. Chem. Int. Ed.* **2012**, *51*, 9935 – 9940

3. V. Hornak, R. Abel, A. Okur, B. Strockbine, A. Roitberg, C. Simmerling, *Proteins* **2006**, *65*, 712 – 725

4. J. Wang, R. M. Wolf, J. W. Caldwell, P. A. Kollman, D. A. Case, *J. Comput. Chem.* **2004**, *25*, 1157 – 1174

5. C. I. Bayly, P. Cieplak, W. Cornell, P. A. Kollman, *J. Phys. Chem.* **1993**, *97*, 10269 – 10280

6. T. Laino, F. Mohamed, A. Laio, M. Parrinello, *J. Chem. Theory Comp*. **2005**, *1*, 1176 – 1184

7. J. VandeVondele, M. Krack, F. Mohamed, M. Parrinello, T. Chassaing, J. Hutter *Comp. Phys. Comm*. **2005**, *167*, 103 – 128

8. V. I. Anisimov, J. Zaanen, O. K. Andersen, *Phys. Rev. B* **1991**, 44, 943 – 954

9. V. Anisimov, F. Aryasetiawan, A. Lichtenstein, *J. Phys. Condens. Matt.* **1997**, *9*, 767 – 808

10. W. E. Pickett, S. C. Erwin, E. C. Ethridge, *Phys. Rev. B* **1998**, *58*, 1201 – 1209

11. J. Perdew, K. Burke, M. Ernzerhof, *Phys. Rev. Lett.* **1996**, *77*, 3865 – 3868

12. J. VandeVondele, J. Hutter, *J. Chem. Phys*. **2007**, *127*, 114105

13. S. Goedecker, M. Teter, J. Hutter, *Phys. Rev. B,* **1996**, *54*, 1703 – 1710

14. C. Hartwigsen, S. Goedecker, J. Hutter, *Phys. Rev. B,* **1998**, *24*, 3641 – 3662

15. S. Nosé, *J. Chem. Phys*. **1984**, *81*, 511 – 519

16. S. Nosé, *Mol. Phys*. **1984**, *52*, 255 – 268

17. W. Hoover, *Phys. Rev. A*. **1985**, *31*, 1695 – 1697

18. B. L. Trout, M. Parrinello, *Chem. Phys. Lett*. **1998**, *288*, 343 – 347

19. B. L. Trout, M. L. Parrinello, *Phys. Chem. B*. **1999**, *103*, 7340 – 7345

20. M. Sprik, *Chem. Phys. Elsevier* **2000**, *258*, 139 – 150

21. J.-P. Ryckaert, G. Ciccotti, H. J. C. Berendsen, *J. Comput. Phys*. **1977**, 23, 327 – 341

22. T. Mülders, P. Krüger, W. Swegat, J. Schlitter, *J. Chem. Phys*. **1996**, *104*, 4869 – 4870.

23. W. K. den Otter, W. J. Briels, *J. Chem. Phys*. **1998**, 109, 4139 – 4146

24. M. Sprik, G. Ciccotti, *J. Chem. Phys.* **1998**, *109*, 7737 – 7744

25. E. A. Carter, G. Ciccotti, J. T. Hynes, R. Kapral, *Chem. Phys. Lett*. **1989**, *156*, 472 – 477

26. C. J. Cramer, D. G. Truhlar, *Phys. Chem. Chem. Phys.* **2009**, *11*, 10757 – 10816

27. L. J.Noodleman, *Chem. Phys.* **1981**, *74*, 5737

28. M. Orio, D. A. Pantazis, T. Petrenko, and F. Neese, *Inorg. Chem.* **2009**, *48*, 7251–7260